Sujal Bista
Institute for Advanced Computer Studies,
Department of Computer Science,
University of Maryland,
College Park, MD 20742
e-mail: sujal@cs.umd.edu

Sagar Chowdhury
Research Assistant
Department of Mechanical Engineering,
University of Maryland,
College Park, MD 20742
e-mail: sagar353@umd.edu

Satyandra K. Gupta
Professor
Fellow of ASME
Institute for Systems Research,
Department of Mechanical Engineering,
University of Maryland,
College Park, MD 20742
e-mail: skgupta@umd.edu

Amitabh Varshney
Professor
Institute for Advanced Computer Studies,
Department of Computer Science,
University of Maryland,
College Park, MD 20742
e-mail: varshney@cs.umd.edu

Using GPUs for Realtime Prediction of Optical Forces on Microsphere Ensembles

Laser beams can be used to create optical traps that can hold and transport small particles. Optical trapping has been used in a number of applications ranging from prototyping at the microscale to biological cell manipulation. Successfully using optical tweezers requires predicting optical forces on the particle being trapped and transported. Reasonably accurate theory and computational models exist for predicting optical forces on a single particle in the close vicinity of a Gaussian laser beam. However, in practice the workspace includes multiple particles that are manipulated using individual optical traps. It has been experimentally shown that the presence of a particle can cast a shadow on a nearby particle and hence affect the optical forces acting on it. Computing optical forces in the presence of shadows in real-time is not feasible on CPUs. In this paper, we introduce a ray-tracing-based application optimized for GPUs to calculate forces exerted by the laser beams on microparticle ensembles in an optical tweezers system. When evaluating the force exerted by a laser beam on 32 interacting particles, our GPU-based approach is able to get a 66-fold speed up compared to a single core CPU implementation of traditional Ashkin's approach and a 10-fold speedup over the single core CPU-based implementation of our approach. [DOI: 10.1115/1.4023862]

1 Introduction

An optical tweezers system is a scientific instrument that uses light to manipulate micron-sized particles. Ashkin first introduced the system in 1986 [1]. Since then scientists have been using this system to manipulate and study microparticles such as dielectric spheres, cells, DNA, bacteria, and virus. They are often used in creating assembly of micro- and nano-scaled components to make a functional device due to the extensive range of positioning and orienting capabilities of the system [2]. Additionally, optical tweezers systems can be used to manipulate cells in a controlled manner without causing them any damage [3–7].

The optical tweezers system is composed of a very powerful laser beam that has a Gaussian-based intensity distribution and a convex lens that focuses the laser beam onto the focal point as shown in Fig. 1. This focused laser beam is used to move microparticles that are submerged in the fluid. When the microparticles are larger than the wavelength of the light used in the laser beam, the ray optics model is used to define the behavior of the optical tweezers system [1]. The laser beam is decomposed into a bundle of rays, each carrying a photon. When these rays interact with the microparticles, they get reflected and refracted. As each ray consists of a photon, the change in the momentum gives rise to the optical force that is exerted on the microparticles. This force is used by the optical tweezers system to trap and move the microparticles. Figure 2 shows an illustration of a microparticle getting trapped. Figure 3 shows a series of images captured through the imaging device in the optical tweezers system in our lab showing a microparticle (silica bead) getting trapped. An optical trap is placed close to the microparticle which exerts a strong gradient force that pulls the particle towards the focal point.

Simulation plays an important role in understanding the optical tweezers system. To manipulate microparticles precisely, the force exerted by the laser has to be known; this is studied by performing simulations. The force calculation is a computationally intensive task because it includes simulation of the Brownian motion of the fluid-suspended microparticles requiring simulation fidelity finer than 10^{-6} s. The popular approach to overcome this timing constraint is to use a precomputed force look-up table to study simulation as done by Banerjee et al. [2]. Reasonably accurate theory and computational models exist for predicting optical forces on a single particle in the close vicinity of the Gaussian laser beam. However, in practice the workspace includes multiple particles that are manipulated using individual optical traps. Experiments have shown that the presence of a particle can cast a shadow on a neighboring particle and hence affect the optical forces acting on it. When microparticles are closely placed under several laser beams, the rays get reflected and refracted which introduces secondary forces that affect the trapping. This behavior is often referred to as shadowing phenomenon. It occasionally causes trapped microparticles to escape or an unwanted microparticle to jump into the trap. Studying this phenomenon is vital for scientists who are using the optical tweezers system for micro assembly or path planning [9–14].

In this paper, we present an optimized GPU-based ray tracing application to calculate the force exerted by the laser beams on the microparticles to study the shadowing phenomenon. Our program is capable of computing the forces exerted by laser beams

Contributed by the Computers and Information Division of ASME for publication in the Journal of Computing and Information Science in Engineering. Manuscript received February 2, 2013; final manuscript received February 19, 2013; published online April 25, 2013. Editor: Bahram Ravani.

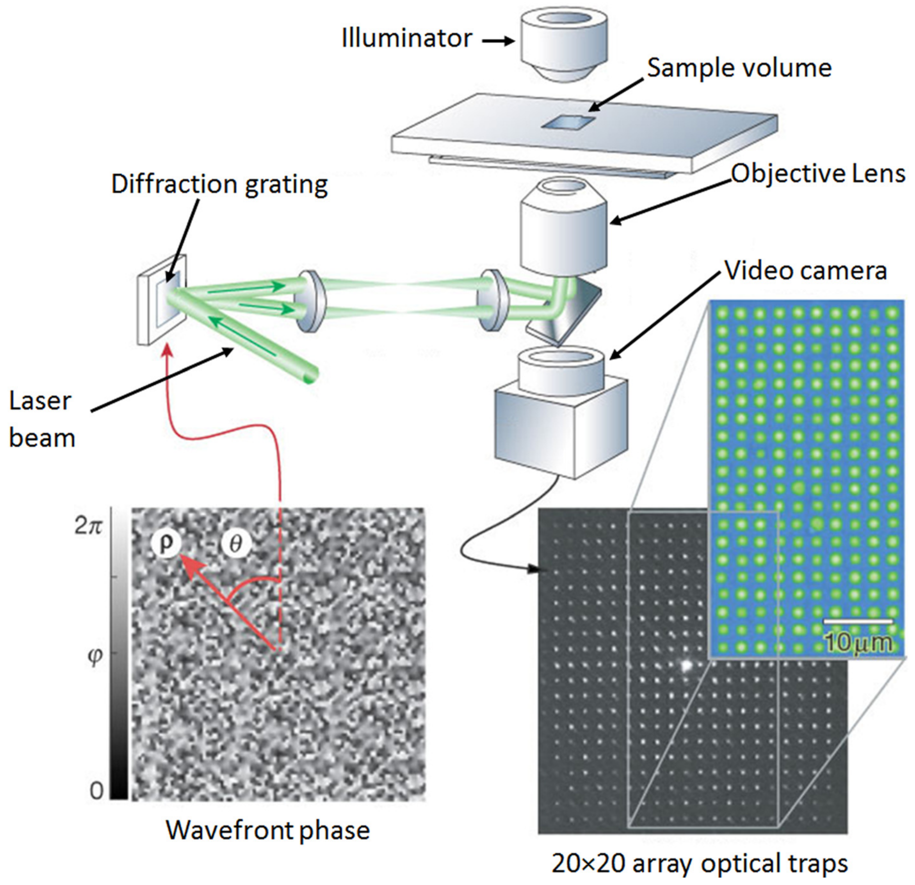

Fig. 1 In an optical tweezer setup, a Gaussian laser beam is converged by a convex lens (objective lens of a microscope) to a focal point which is used for trapping microparticles. To create multiple optical traps, the laser beam is split into multiple-beams using a diffraction grating. Diagram courtesy of [8].

on multiple microparticles (up to 32) at more than 100 Hz, which is faster than the rate at which a typical optical device would image/monitor the microparticles. We are able to calculate the interaction between the lasers and several microparticles to study the shadowing phenomenon vital for understanding optical trapping. When evaluating the force exerted by a laser beam on 32 interacting particles, our GPU-based approach is able to get approximately a 66 times speed up compared to a single core CPU implementation of traditional Ashkin's approach and 10 times speedup over our approach's CPU implementation. In this paper, we also talk about several choices we made while developing this application and compare them in terms of performance and precision. We also present an alternative way to calculate force exerted by the laser that exploits coherence of the mapping from incident ray to the x,y,z components of the force and the transmitted ray by using non-negative matrix factorization (NMF). This method is useful when the ray's path within the microparticle cannot be easily computed by simple sphere-object intersections (possibly caused by uneven density of the microparticle). We also present an instance where the shadowing effect drastically changes the amount of force applied on a microparticle.

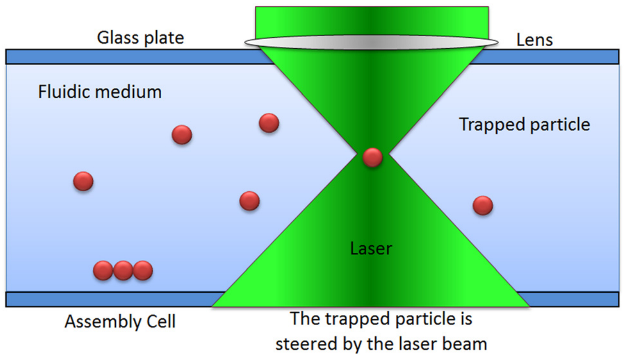

Fig. 2 An illustration of the optical tweezers system. A laser beam with a Gaussian-based intensity distribution is converged into a focal point with the help of a convex lens. The figure shows laser beam trapping microparticles at the focal point.

2 Related Work

Powerful lasers are used to manipulate microparticles in an optical tweezers system. This was first introduced by Ashkin et al. [15], where a single-beam gradient force was used to trap micro- and nano-sized dielectric particles. Ashkin later introduced a geometric ray-optics model that is used to compute trapping forces created by a laser acting on microparticles much larger than the wavelength of light [1]. Though the equation Ashkin used is fairly optimized as it computes scattering and gradient forces based only on the incident angle and the radial position of the ray, it only works with rigid spherical objects and cannot be used directly to study interaction between several beams and microparticles. Our work is focused on calculating forces using our GPU-based ray tracing algorithm which provides both speed and flexibility needed to study shadowing phenomenon.

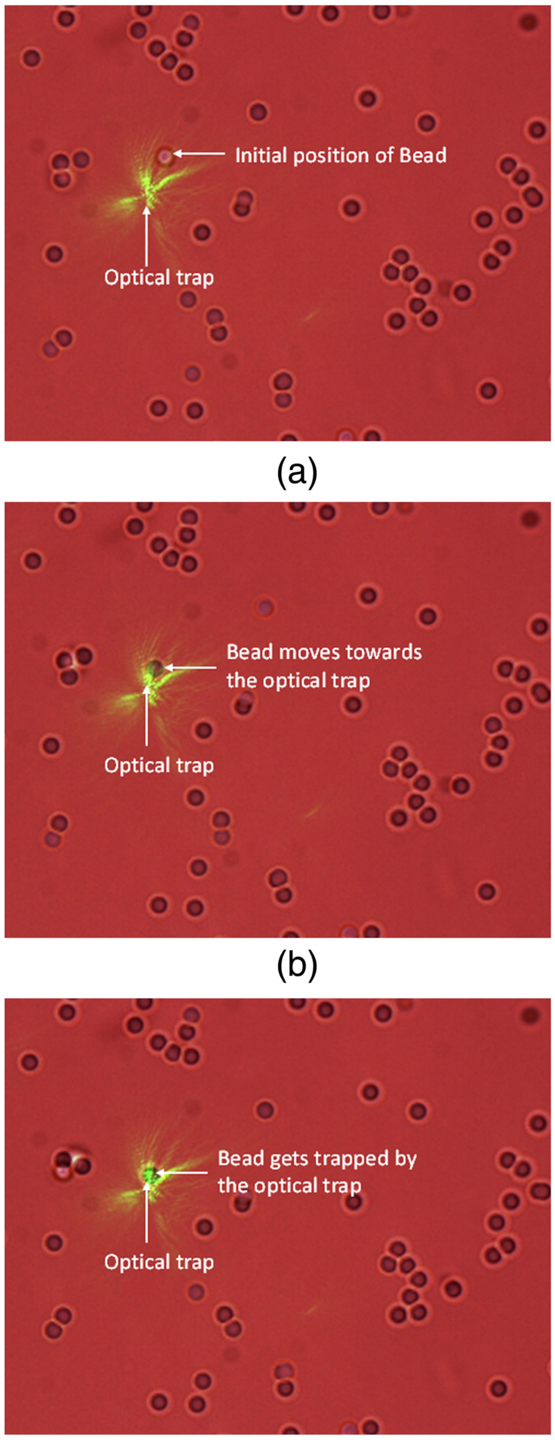
Initial position of Bead
Optical trap
(a)
Bead moves towards the optical trap
Optical trap
(b)
Bead gets trapped by the optical trap
Optical trap
(c)

Fig. 3 When an optical trap is placed close to a microparticle, it pulls the particle towards the focal point. The images above captured using the imaging device in the optical tweezers system show a microparticle moving into a trap.

One of the biggest challenges in simulating the optical tweezers system is efficiently performing calculation of the laser force calculation. Since the microparticles are influenced by the Brownian motion, simulations have to be done at a time scale much smaller than a microsecond. Banerjee et al. [2] introduced a framework where offline simulation is used to precompute data at discrete points and is later used to perform fast and accurate calculation of dynamic trapping probability estimates at any arbitrary point in 3D. This approach cannot accurately compute the effect when laser interacts with several nanoparticles. We focus on calculating the force quickly on dynamic microparticles so that the interactions of laser with several microparticles can be accurately simulated to study the shadowing phenomenon.

Bianchi and Leonardo [16] use GPUs to perform optical manipulation using holograms in real-time. They achieved speedups of 45× and 350× over CPU on their super position algorithm (SR) and Gerchberg-Saxton weighted algorithm (GSW), respectively. The speedup helped them to perform interactive micromanipulation. Balijepalli et al. [17] and Patro et al. [18] have used GPUs to compute trapping probabilities and have gotten significant speedups. Our approach in this paper can work on CPUs and GPUs. We perform ray tracing to compute the force exerted by the laser as it interacts with several microparticles.

Sraj et al. [19] used dynamic ray tracing to deduce the optical force on the surface of the deformable cell from which they calculate stress distribution. Rather than using the rigid spheres as an approximated shape of the cell, they perform force calculation on the actual cell. They show that the shape of the cell strongly influences how the optical force stretches and deforms them. They also highlight that the applied optical forces change drastically when the cells are deformed. We focus our efforts on reducing the amount of time required to compute the exerted force. We perform our calculation on rigid microparticles and study how optical forces change when laser interacts with several nanoparticles that are closely interacting with each other.

Zhou et al. [20] have introduced a force calculating model that uses ray tracing based on spatial analytic geometry. In our ray-tracing-based approach we perform GPU-based optimizations and calculate interaction of laser beams with multiple particles efficiently which is critical to studying the shadowing phenomenon. We also provide an alternative way of computing the forces using NMF.

Using GPUs to accelerate computationally expensive algorithms is gaining a strong interest in the scientific and gaming community. Early work done by Harris et al. [21] used GPUs to perform visual simulation of fluids, clouds, and smoke. They mapped some basic operators (like heat and Laplace) on the GPU and used these operators to accelerate the simulation. They performed their calculation on the GPU using programmable shaders before general languages for GPU like CUDA, DirectX Compute, and OpenCL became prominent. Considerable advancements in physically-based simulation have been made recently due to their application in games and graphics [22]. In particular, fluid simulations on GPUs have gained significant momentum [23–26]. Recently, Phillips et al. [27] used a cluster of GPUs to accelerate solver for 2D compressible Euler equation and MBFLO solvers. Using a cluster of 16 GPUs they achieve speedups of 496× and 88× on their Euler and MBFLO solvers. The trend of using GPUs to accelerate existing algorithms is growing. In our work, we use GPU-based accleration of ray tracing to compute the force exerted by the optical tweezers on the microparticles.

Carr et al. [28] make a persuasive case for the use of GPUs for computing ray-triangle intersections efficiently by using pixel shaders. Purcell et al. [29] mapped the complete ray tracing algorithm to the GPUs, using different pixel shaders for creating rays, traversing rays, intersecting rays with triangles, and illumination calculations. Our ray tracing program to NVIDIA's Optix but rather than calculating color per pixel we compute the force exerted by the laser beam on the microparticles and perform integration. Also, the density of rays and the paths taken by the rays used in our calculation are different from the ones used by a typical ray tracing program that uses a pinhole camera model.

3 Approach

A simplified ray-optics model for calculating the force is shown in Fig. 4. Due to the change in the index of refraction between the fluid and the microparticle, the incident ray is diverted from its

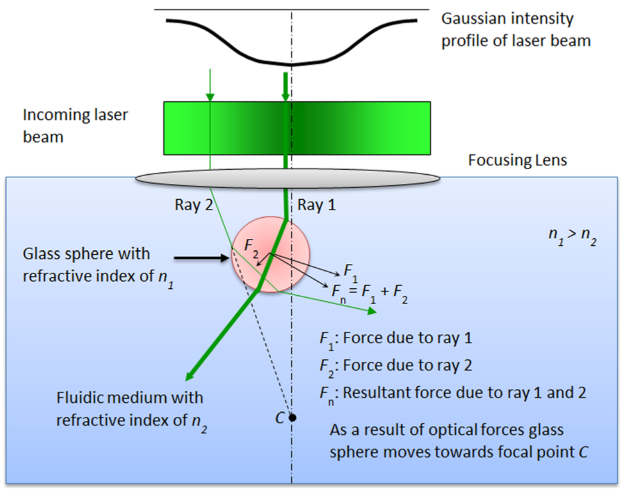

Gaussian intensity profile of laser beam
Incoming laser beam
Focusing Lens
Ray 2
Ray 1
$n_1 > n_2$
Glass sphere with refractive index of n_1
F_2
F_1
$F_n = F_1 + F_2$
F_1: Force due to ray 1
F_2: Force due to ray 2
F_n: Resultant force due to ray 1 and 2
Fluidic medium with refractive index of n_2
C
As a result of optical forces glass sphere moves towards focal point C

Fig. 4 Diagram showing the simplified ray-optics model for calculating the force. The incident ray is diverted from its original path when it interacts with the microparticle. This causes the ray to change its momentum. When the ray changes momentum due to the microparticle, equal and opposite force is applied to the microparticle.

original path as it goes through the microparticle. This causes the ray to change its momentum. When the ray changes momentum, equal and opposite force is applied to the microparticle. We calculate force contributed by each ray for each particle. After the contribution of each ray is calculated, integration is done to find the total force. We divide the entire force calculation process into several steps described below.

3.1 Ray-Object Intersection. We compute ray-object intersection on the GPU using a 3D-grid-based data structure. We choose a uniform grid-based data structure over BSP, kDTree, and Octree because creating, updating, and ray traversing operations are faster due to the constant time access to the cells and the use of the efficient 3D-DDA algorithm for ray-traversal [29,30]. In our application, the grid-based data structure is created on the CPU and sent to the GPU memory every frame. In the optical tweezers system, the number of particles monitored in the experiments is often less than 64, so we create and update the data structure on the CPU. Once the grid data is transferred to the GPU, we perform ray-object intersection using a GPU kernel. The ray-object intersection is highly parallelizable and a significant performance gain is achieved by using the massively parallel cores of a GPU as compared to a single core of a CPU. At first we considered using Optix for ray tracing. However we soon realized that we needed a ray tracer that was more flexible to meet our memory mapping needs, easily integrable with the further steps in the force calculation pipeline, and incurred less overhead. As Optix is a general-purpose ray tracing software made for rendering, we decided to develop our own dedicated GPU-based program that is highly specialized for force calculation.

The laser beams are decomposed into R_N rays. Each ray is mapped to a thread in the CUDA kernel and all R_N threads are launched at the same time. We save the attributes (such as position, radius) of the microparticles and the 3D grid data in the global GPU memory whereas the properties of the 3D grid and the laser beam are saved in the constant GPU memory as shown in Fig. 5. Every thread traces the path of a ray independently.

3.2 Force Calculation. When a ray intersects a microparticle, we compute the reflected, refracted, and the final transmitted ray by performing basic intersections. Using these rays and the properties of the microparticle, we first compute only the

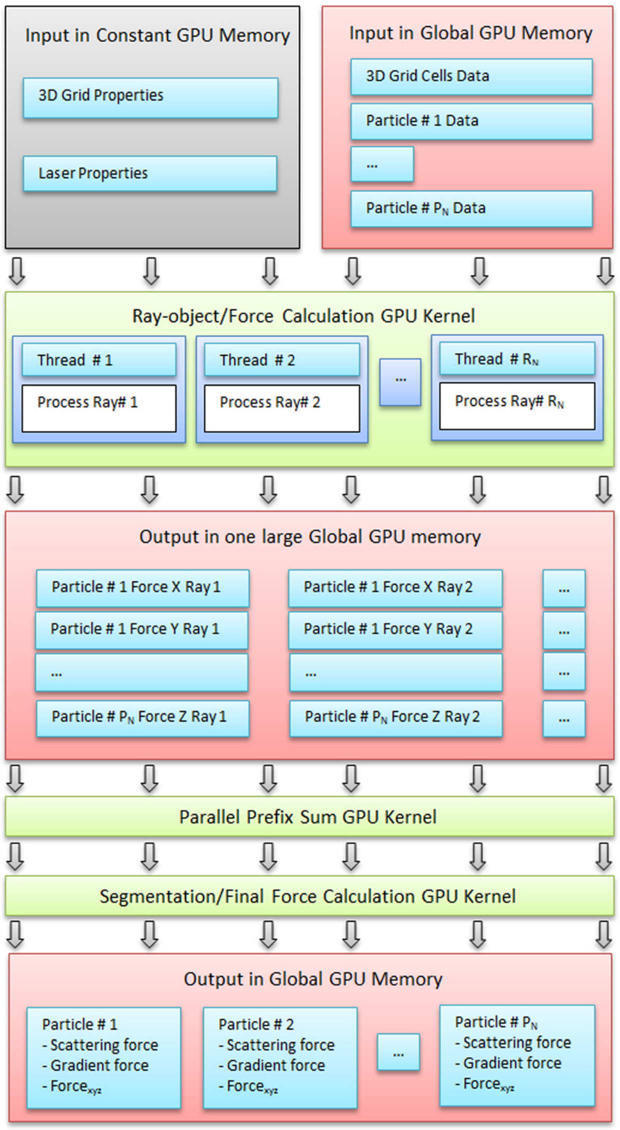

Input in Constant GPU Memory
3D Grid Properties
Laser Properties
Input in Global GPU Memory
3D Grid Cells Data
Particle # 1 Data
...
Particle # P_N Data
Ray-object/Force Calculation GPU Kernel
Thread # 1
Process Ray# 1
Thread # 2
Process Ray# 2
...
Thread # R_N
Process Ray# R_N
Output in one large Global GPU memory
Particle # 1 Force X Ray 1
Particle # 1 Force Y Ray 1
...
Particle # P_N Force Z Ray 1
Particle # 1 Force X Ray 2
Particle # 1 Force Y Ray 2
...
Particle # P_N Force Z Ray 2
...
Parallel Prefix Sum GPU Kernel
Segmentation/Final Force Calculation GPU Kernel
Output in Global GPU Memory
Particle # 1 - Scattering force - Gradient force - Force$_{xyz}$
Particle # 2 - Scattering force - Gradient force - Force$_{xyz}$
...
Particle # P_N - Scattering force - Gradient force - Force$_{xyz}$

Fig. 5 An overview of the GPU pipeline. The properties of the laser and the 3D grid are saved into the constant GPU memory, whereas the properties of the particles and the 3D grid cells are saved in the global GPU memory. These are used by the first GPU kernel that performs ray-object intersection and force per ray calculation. The output is written to a large global memory array. We then perform a parallel-prefix sum at the output. As the parallel-prefix sum adds up all the components together, segmentation/final force calculation kernel finds the proper segment boundaries for each component and subtracts necessary amount from the boundaries to compute the final result.

magnitude of the scattering and the gradient force using the equation described by Ashkin [1],

$$F_s = \frac{n_1 P}{c}\left\{1 + R\cos(2\theta) - \frac{T^2[\cos(2\theta - 2r) + R\cos(2\theta)]}{1 + R^2 + 2R\cos(2r)}\right\}$$

$$F_g = \frac{n_1 P}{c}\left\{R\sin(2\theta) - \frac{T^2[\sin(2\theta - 2r) + R\sin(2\theta)]}{1 + R^2 + 2R\cos(2r)}\right\}$$

where n_1 is the index of refraction of the incident medium, c is the speed of light, P is the incident power of the ray, R is the Fresnel reflection coefficient, T is the Fresnel transmission coefficient, θ is the angle of incidence, and r is the angle of refraction. Then we

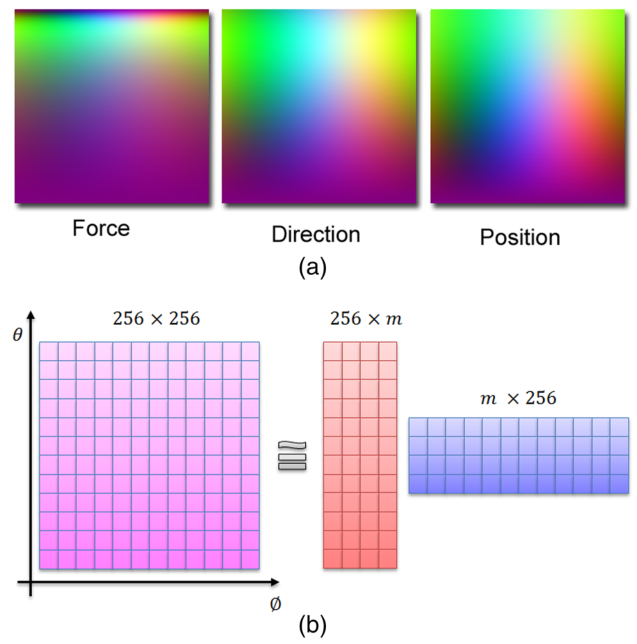

Fig. 6 Pictorial view of the matrices that map discretized representation of incident ray angles to the force applied to the microparticle, the direction of the transmitted ray, and the position of the transmitted ray. The mapping is highly coherent which allows NMF to efficiently factorize each component of the matrix into two compact sized outer product matrices. Value of *m* used in our experiments is 4.

compute the direction of the scattering and the gradient forces directly from the vectors obtained from ray tracing. The direction of the ray is the same as the scattering direction. For the gradient direction, we use the scattering direction's orthogonal component that lies on the plane formed by the center of the particle, the point where the ray intersects the particle, and the intersection of the ray with the horizontal plane as described in [1,20]. Now using the computed magnitude and the direction, we find the scattering and gradient forces. These forces are combined to calculate the total force exerted by the ray. The total force is then saved in the GPU memory. The transmitted ray is further traced to find the intersection of the ray with other particles and the steps described above are repeated as needed.

3.3 Force Calculation Using Non-Negative Matrix Factorization. As an alternative to calculating the force independently for each ray, we also use non-negative matrix factorization (NMF) to take advantage of the coherence between the input rays, the force exerted, and the transmitted rays. The idea is to rotate the ray-object intersection point so that it lines up with the axis-aligned pole of the microparticle. Then we represent the ray by its spherical coordinates. We discretize the angles, compute the force exerted, and the outgoing transmitted ray for each discrete set of angles. This provides us a look-up map that is used to convert the incident ray angle to the exerted force, outgoing ray position, and direction directly. This look-up map can be very large and is generated for each component of the force and the outgoing ray. We have observed that there is a high coherence between the mapping of the exerted force and the transmitted rays as shown in Fig. 6(*a*). To take advantage of this coherence, we use NMF to factorize each mapping matrix into two compact matrices. Lawrence et al. [31] have applied NMF to decompose the reparameterized BRDF matrix that uses the half angle formulation. Here, we use NMF to compact the mapping matrix as shown in Fig. 6(*b*).

Once the matrices are saved, computing the force exerted by a ray is straightforward. When a ray intersects a sphere, we first

Table 1 The time in seconds taken by the various methods to compute total force exerted on a single microparticle performed 5000 times at different locations

	Number of rays					
Method	8^2	16^2	32^2	64^2	128^2	256^2
Ashkin (Float)	0.0759	0.3558	1.2708	5.0548	20.2793	81.7446
Ashkin (Double)	0.0762	0.3705	1.3399	5.3316	21.5276	86.5138
CPU Ray (Float)	0.0807	0.3389	1.4369	5.4946	22.1243	88.9347
CPU Ray (Double)	0.0852	0.3529	1.4268	5.7644	22.8563	92.5199
GPU NMF (Float)	0.9592	0.9589	0.9826	1.1923	2.0615	5.4888
GPU Ray (Float)	0.7132	0.8745	0.8337	0.9007	1.2058	2.3813

compute the intersection position and the incident direction. We rotate the ray so the intersection position aligns with the pole of the microparticles. We then convert the incident ray into spherical coordinates. Using these angles, we multiply the appropriate rows and columns of the matrices generated by the NMF to get the mapping for each component of the force and the transmitted ray. Once we have the components, we apply inverse of the rotation that we applied to the incident ray to then calculate final values.

By using this alternative method to compute the force, we can take advantage of the coherence of the mapping. However, this method suffers from performance and precision issues compared to the ray tracing approach. The performance loss is caused by the matrix multiplication to rotate the vectors and the cost of multiplying a row and a column to get values for each component of the force and the transmitted ray. The performance results are shown in Table 1. The precision loss is created by discretization of the input angles and the compact factorization created by NMF. Due to these reasons, we use regular Ashkin's equation to calculate force using ray tracing when the micro-sphere is used. However we believe that the NMF method can be useful when the microparticle has an uneven density which makes computation of the path a ray travels within the particle both difficult and computationally expensive. Such cases arise when computing the force applied to cells or nonhomogeneous micro-spheres with nonuniform density distribution.

3.4 Force Integration. Once the CUDA kernel to compute the force for each ray is completed, we compute the net force applied on each particle by performing integration of the force field over the surface of the microparticle as done by Banerjee et al. [2]. We also perform this calculation on the GPU to save data transfer latency. At this stage of the pipeline, we have the force exerted by each ray in the GPU memory. Each component of the force for each particle is grouped and saved in a different part of a single large memory array. For example, all the scattering force exerted on a particle is saved in the first block followed by the gradient force and then followed by the entries of the second particle as shown in Fig. 5. We perform a parallel-prefix sum on this large array. This will scan all the components of the force for all particles together. Since the number of particles and the individual values of the force components used in the simulation are small, we do not suffer overflow error while performing the parallel-prefix sum. We then execute another CUDA kernel that segments and outputs the final force contribution for each particle by subtracting appropriate entries from the segment boundaries of each component as shown in Fig. 7. This final step performs extremely well on the GPU because the output of the previous step is large and so transferring it to the CPU will incur a large latency. By calculating the final force contribution directly on the GPU, we only need to read back the several components per particle.

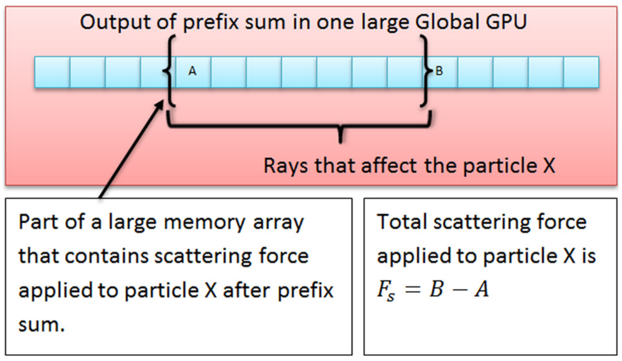
Output of prefix sum in one large Global GPU
A
B
Rays that affect the particle X
Part of a large memory array that contains scattering force applied to particle X after prefix sum.
Total scattering force applied to particle X is $F_s = B - A$

Fig. 7 The final force contribution for each particle is calculated by subtracting values from the segment boundaries of an array that contains the result of the parallel-prefix sum. In this figure, we show how the final value of the scattering force is computed for a particle.

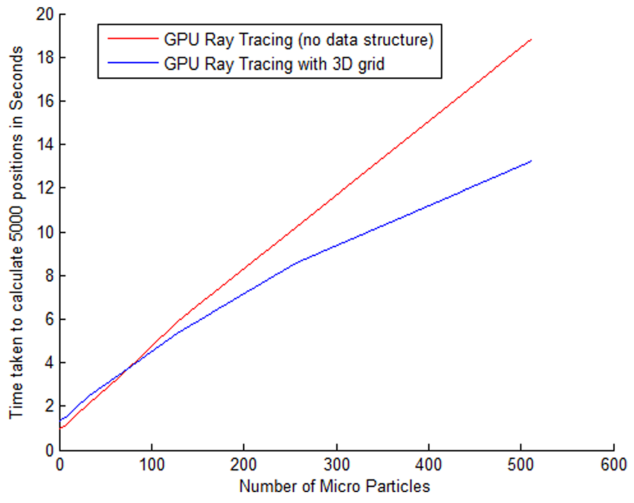

Fig. 8 Here we show the time taken to compute the force exerted by a laser beam containing 32 rays 5000 times on a varying number of particles. We compare brute-force GPU ray tracing against GPU ray tracing with a 3D grid. As the number of particles increases, the use of a 3D grid data structure shows a clear advantage.

4 Results and Discussion

We have implemented our system in C++. We use the CUDA API for the GPU-based ray tracing. For all of our experiments, we use Windows 7 64-bit machine with Intel I5-750 2.66 GHz processor, NVIDIA GeForce 470 GTX GPU, and 8 GB of RAM.

4.1 Performance Comparison. We first show the performance gains achieved by using our GPU-based method. In our first set of experiments, we use rigid microparticles and record the amount of time it takes to compute the force. Our performance results are shown in Tables 1 and 3. We compare the timings of various methods: Ashkin's traditional, CPU-based ray tracing, GPU-based method that uses NMF, and GPU-based ray tracing methods using single and double precision floating-point arithmetic. For the first experiment, we performed force calculations on a single microparticle 5000 times placed at different locations around the focal point of the laser beam. We also varied the number of rays that are used to describe the laser beam. As shown in Table 1, when only one microparticle and 256^2 rays are used to represent the laser beam, the GPU-based force calculation is about 34 times faster than Ashkin's method.

We compare precision among CPU- and GPU-based implementations of our approaches against CPU-based Ashkin's method

Table 2 Here we show the comparison of precision between various methods rounded up to the nearest four digits. We take Ashkin's method as the reference and compute the relative error to compare other methods with an equal number of rays. As the number of rays increase, the relative error decreases in general but the computational cost increases.

	Number of rays						
Method	8^2	16^2	32^2	64^2	128^2	256^2	512^2
GPU NMF (Float)	0.0068	0.0047	0.0034	0.0028	0.0035	0.0025	0.0032
CPU Ray (Double)	0.0001	0.0001	0.0001	0.0001	0.0001	0.0001	0.0001
CPU Ray (Float)	0.0005	0.0001	0.0001	0.0001	0.0002	0.0001	0.0001
GPU Ray (Float)	0.0005	0.0006	0.0005	0.0005	0.0005	0.0005	0.0005

Table 3 The time taken (in s) by the various methods to compute total force exerted by a laser beam on 32 interacting microparticles computed 5000 times at different locations. It is interesting to note that when the number of rays is low, brute-force ray tracing is faster than the ray tracing method that uses a 3D grid data structure. This is due to the additional cost of creating and maintaining the data structure.

	Number of rays					
Method	8^2	16^2	32^2	64^2	128^2	256^2
Ashkin (Float)	1.8877	7.7762	31.5119	128.1370	515.1390	2081.6000
Ashkin (Double)	1.7971	7.7572	32.0977	129.2160	519.8880	2101.7000
CPU Ray (Float)	0.2951	1.2400	5.1456	21.4900	86.4165	346.2620
CPU Ray (Double)	0.3103	1.3025	5.9534	23.8178	95.1179	379.2980
CPU Ray with 3D Grid (Double)	0.3831	1.3404	5.7862	22.8523	90.7224	360.8080
GPU NMF (Float)	1.3050	2.0442	3.5816	9.1022	30.7739	116.5450
GPU Ray (Float)	1.2649	1.6148	1.9824	3.7576	9.9187	33.3911
GPU Ray with 3D Grid (Float)	1.8859	1.8621	2.2662	3.6953	9.4589	31.5070

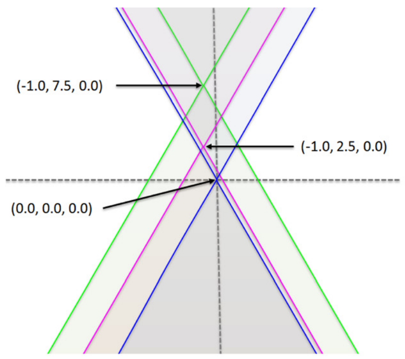

(a) Focal point of three laser beams

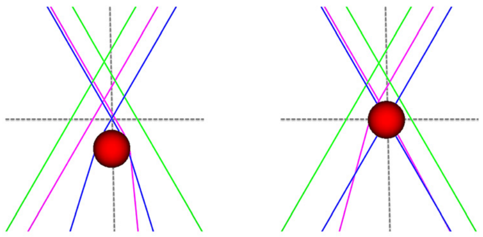

(b) Single microparticle moving in Y axis

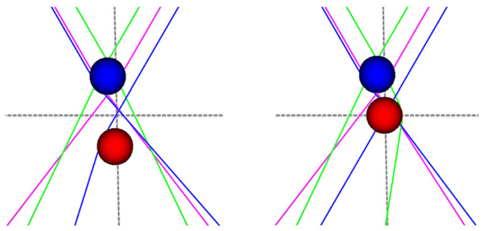

(c) Multiple microparticle with one bead moving in Y axis

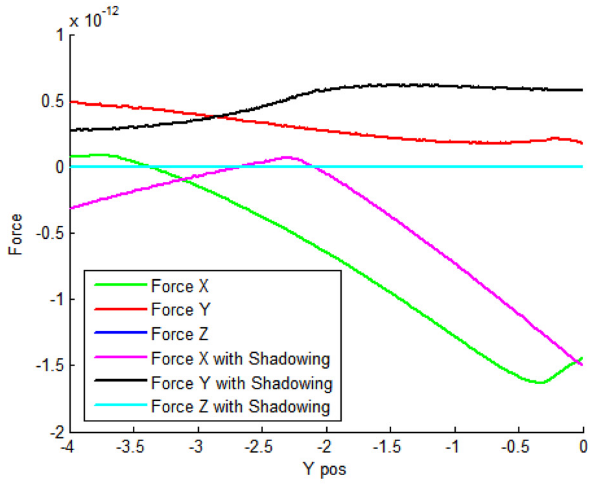

(d) Force comparision

Fig. 9 An illustration of the shadowing phenomenon. (*a*) shows the focal point of three laser beams at location $(0.0, 0.0, 0.0)$, $(-1.0, 7.5, 0.0)$, and $(-1.0, 2.5, 0.0)$. (*b*) shows the movement of a single particle from $(0.0, -4.0, 0.0)$ to $(0.0, 0.0, 0.0)$. (*c*) shows the movement of same particle when second particle is present at location $(-1.0, 5.5, 0.0)$. Finally, (*d*) shows the difference in force experienced by the first bead caused by the shadowing phenomenon.

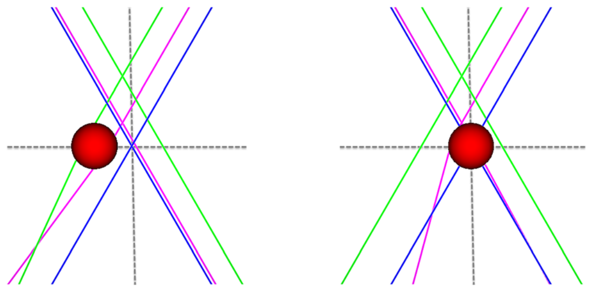

(a)

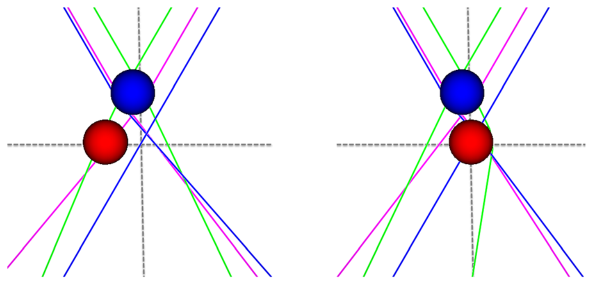

(b)

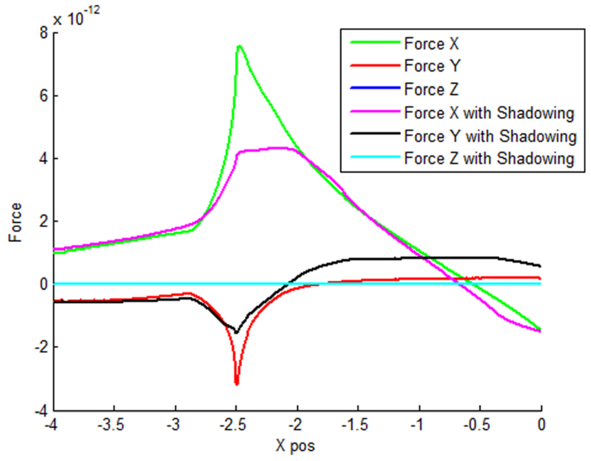

(c)

Fig. 10 An illustration of the shadowing phenomenon similar to the previous figure. (*a*) shows the movement of a single particle from $(-4.0, 0.0, 0.0)$ to $(0.0, 0.0, 0.0)$. (*b*) shows the movement of same particle when second particle is present at location $(-1.0, 5.5, 0.0)$. Finally, (*c*) shows the difference in force experienced by the first bead caused by the shadowing phenomenon.

using equal number of rays and double-precision floating-point arithmetic. We perform several comparisons by varying the number of rays to represent the laser beam. The results are shown in Table 2. In general, the relative error decreases as the number of rays increases. For NMF based computation, the relative error decreases at first and then fluctuates slightly as we increase the number of rays. This is because we discretized input angles while creating the mapping table. Due to this, increasing the number of rays while keeping the size of the mapping table constant, can increase the amount of error. For regular computations, 32^2 is an ideal number of rays to use to represent the laser as both the relative error and the computation cost are low.

For the second experiment, we performed force calculations using a laser beam and 32 interacting microparticles computed 5000 times placed at different locations. The ray tracing methods can capture the interaction of a laser with multiple particles while Ashkin's traditional method can only capture interaction of the laser with a particle at a time ignoring the shadowing effects. For the second experiment, we also show the performance difference

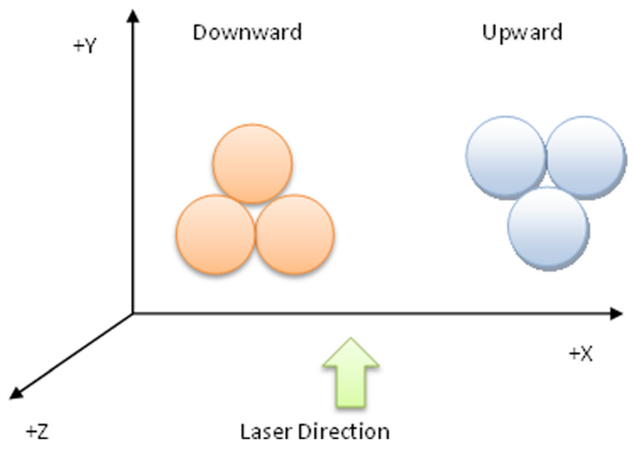

Fig. 11 Here we show the arrangement of the microparticles in the upward and downward configuration

from the use of a spatial data structure while doing ray tracing. As shown in Table 3, GPU-based force calculation that uses grid based data structure is about 66 times faster than traditional Ashkin's method and about 10 times faster than its CPU-based ray tracing analog when 256^2 rays are used to represent the laser beam. As shown in Fig. 8, when the numbers of rays or particles increases, the 3D grid performs better than the brute-force ray tracing method. This is generally because of the overhead of creating, updating, and transferring the grid to the GPU.

4.2 Shadowing Phenomenon. In the traditional ray-tracing community, the phenomenon of multiple refractions we are simulating would be referred to as the second and higher-order refractions. However, since this is referred to as the shadowing phenomenon by the optical tweezers community, this is the term we shall use here.

We use two microparticles for these experiments. The first microparticle moves along a path. The second microparticle is stationary and is gripped by two laser beams with one focal point above and the other below the microparticle. The rays that are incident on the second microparticle get refracted which can influence the number of rays that interact with the first microparticle. Thus the presence of the second microparticle causes a change in the amount of force being applied to the first microparticle. We show this change through simulations.

In the first experiment, we simulate using a single silica bead of size 5 μm. We use three downward pointing Gaussian laser beams focused at locations $(0.0, 0.0, 0.0)$, $(-1.0, 7.5, 0.0)$, and $(-1.0, 2.5, 0.0)$, respectively. A bead is placed at $(0.0, -4.0, 0.0)$ and it slowly moves to $(0.0, 0.0, 0.0)$. In Fig. 9, we show the force experienced by the bead as it goes from $(0.0, -4.0, 0.0)$ to $(0.0, 0.0, 0.0)$.

Now to show the shadowing phenomenon, we add an extra bead at location $(-1.0, 5.5, 0.0)$ in the setup described above. This bead acts like a lens and changes the direction of the rays from the lasers. This causes the first bead to experience force from secondary rays. We compute the force experienced by the bead as it goes from $(0.0, -4.0, 0.0)$ to $(0.0, 0.0, 0.0)$ when the shadowing phenomenon is occurring. In Fig. 9, we show the difference in the amount of force experienced by the first microparticle. This change adds instability and weakens the optical traps. We next repeat the experiment but this time move the bead from $(-4.0, 0.0, 0.0)$ to $(0.0, 0.0, 0.0)$. Figure 10 shows the result of force calculation with and without the shadow phenomenon.

In both experiments, shadowing effects change the applied force significantly. This can change the behavior of the optical traps. Experimentally validating the results of simulations is challenging. There is no direct way to measure force. The force needs to be inferred from the observed motion. This requires a high speed image capture, accounting for the Brownian motion, and accounting for image blurring due to motion in the z-direction. We are currently in the process of designing experiments to record particle trajectories in the presence and absence of shadowing phenomena.

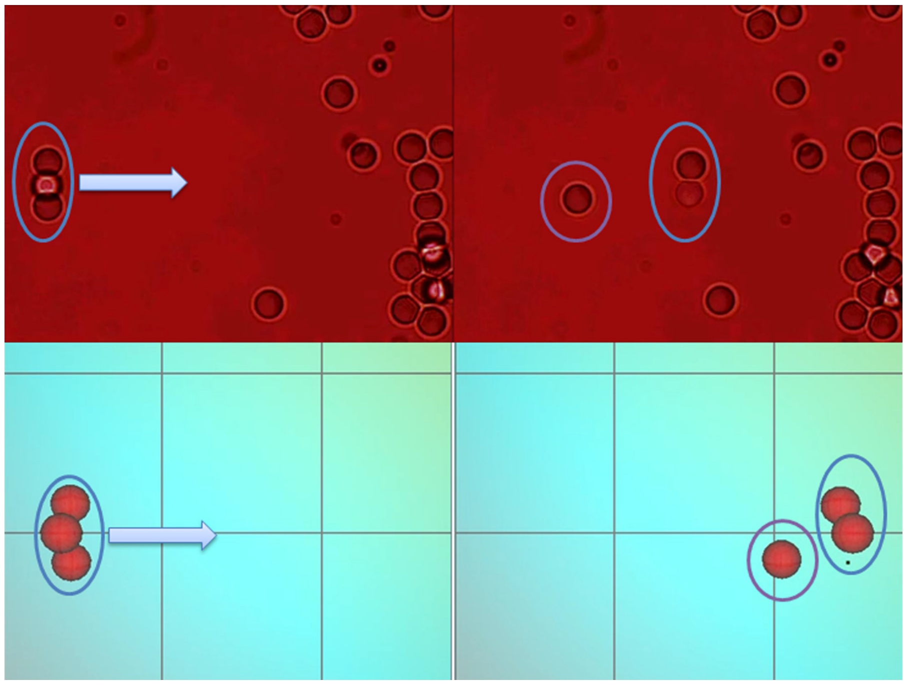

Fig. 12 Downward configuration with spacing 2.5 μm between the lower microparticles and laser moving with the velocity 22.4 μm/s. The two beads are trapped as the laser moves. The top row shows the captured video and the bottom row shows the simulated result.

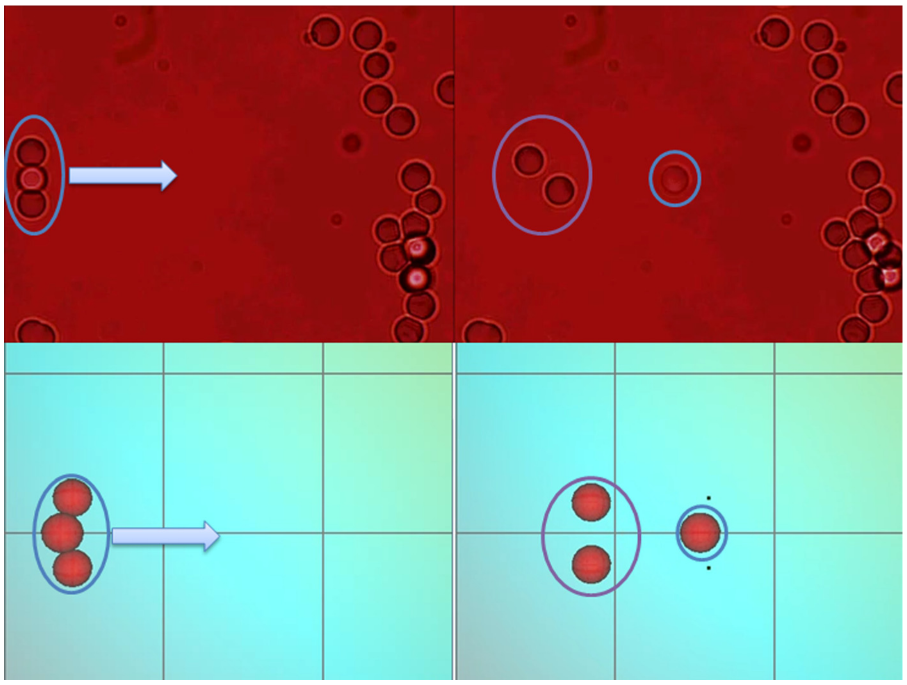

Fig. 13 Downward configuration with spacing 4.0 μm between lower two microparticles and laser moving with the velocity 22.4 μm/s. Only one bead is trapped as the laser moves. The top row shows the captured video and the bottom row shows the simulated result.

4.3 Calibration and Validation. We have calibrated our system by using multiple recorded videos of the holographic optical tweezers system trapping a single freely moving microparticle. The system is calibrated by estimating the laser power at the objective lens by trapping a freely diffusing particle and observing its velocity as it falls into the trap. We used estimated laser power for our simulation. We added a repulsive force acting upward in the positive Y direction in the simulation to model the electrostatic force from the surface that prevents the beads from falling down to the surface. The distance of each microparticle from the bottom of the surface can vary and they can all have different charges, resulting in different amounts of repulsive force. We estimated the repulsive force based on the observed behavior. Using the estimated power of the laser and the estimated repulsive force, we were able to simulate the observed behavior of the microparticles.

Using our calibrated system we analyze the stability of gripper configurations reported in [5]. We are able to successfully predict which microparticles in a particular gripper formation are more likely to jump out of the optical traps due to the shadowing effect when the gripper moves faster than the allowable speed. We consider two different gripper configurations for our analysis. The first configuration has two microparticles trapped above the image plane while the third microparticle is trapped below. In the second configuration, two microparticles are trapped below the image plane while the third one is slightly above. Both configurations are shown in Fig. 11. We consider three different gripper geometries for each type of gripper configuration. For the X-Z distance between microparticles, we use 0.0, 2.5, and 4.0 μm. We analyze the gripper stability for three different velocities, namely 3.8, 15.0, and 22.4 μm/s.

In the upward configuration, all three particles are moved successfully and the configuration is stable. Our simulator is able to accurately reproduce the behavior of the configuration observed in physical experiments.

Downward configuration where the lower beads are in contact with each other can be stably held while transporting at laser trap velocities of 3.8, 15.0, and 22.4 μm/s. On the other hand, the configuration where the beads are 2.5 μm apart is stable only at lower velocities of 3.8 and 15.0 μm/s. One of the lower beads falls behind while transporting with 22.4 μm/s and hence the configuration breaks down (see Fig. 12). However, in case of the configurations with the lower beads separated by 4 μm, only the upper bead can be steered by the laser at 22.4 μm/s (see Fig. 13). The configuration remains stable while transporting with the lower velocities

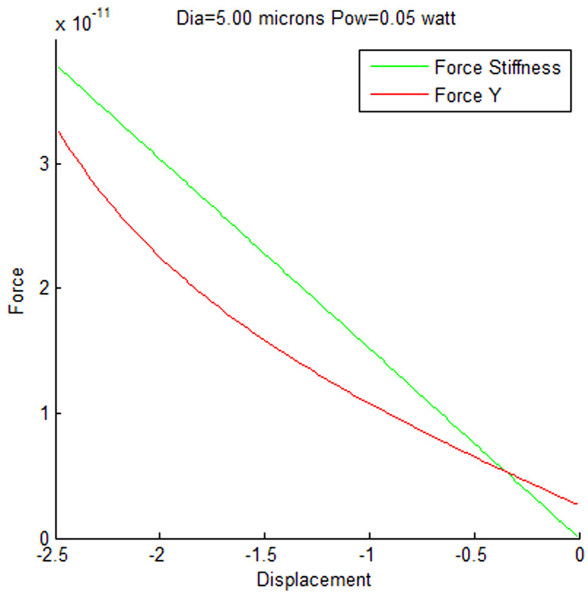

Fig. 14 Here we show the comparison between the force calculated using our method and the force computed using stiffness. Here the focal point of the laser is located at (0.0, 0.0, 0.0) and we compute force by placing the microparticle along the Y-axis. Both forces are similar. The force computed using stiffness is an approximation but we validate our result since the stiffness value computed by Singer et al. [32] is calibrated.

(3.8 and 15.0 μm/s). Our simulation is able to successfully predict the breaking point for the configurations (see Figs. 12 and 13).

We have also compared and validated force calculated using our method against the force computed using stiffness $F = -kd$, where k is the stiffness and d is the displacement distance between the center of the microparticle and the focal point of the laser. Here, we use the stiffness value computed by Singer et al. [32] for a microparticle of diameter 5 μm and the laser with power 0.05 W. In Fig. 14, we show the force computed by both methods when the microparticle is placed at various distances from the focal point. We have found the values to be comparable. Although the force computed using stiffness is an approximation, we have compared and validated our result because the stiffness value computed by Singer et al. [32] is calibrated.

5 Conclusion and Future Work

The GPU-based system we have presented in this paper computes the forces when laser beams interact with multiple microparticles and allow a scientist to study the shadowing phenomenon. Studying these phenomenon in real-time is vital as it allows efficient planning required for trapping and manipulating microparticles. When evaluating the force exerted by a laser beam on 32 interacting particles, our GPU-based application is able to get approximately a 66-fold speed up compared to the single core CPU implementation of traditional Ashkin's approach and 10-fold speedup over our approach's serial CPU implementation. We have also presented an alternative way to calculate the force exerted by the laser that exploits the coherence of the mapping from the incident ray to the components of force and the transmitted ray by using NMF.

In the future we plan to perform experimental investigation to validate our computational model by performing tests on scenarios that can be validated experimentally. Currently every time step is computed independently. Computing the force over a few time steps by efficiently processing the incremental changes might provide further speedup.

Acknowledgment

This work has been supported in part by the NSF Grants No. CCF 04-29753, CNS 04-03313, CCF 05-41120, and CMMI 08-35572. We also gratefully acknowledge the support provided by the NVIDIA CUDA Center of Excellence award to the University of Maryland. Any opinions, findings, conclusions, or recommendations expressed in this article are those of the authors and do not necessarily reflect the views of the research sponsors.

References

[1] Ashkin, A., 1992, "Forces of a Single-Beam Gradient Laser Trap on a Dielectric Sphere in the Ray Optics Regime," Biophys. J., **61**, pp. 569–582.
[2] Banerjee, A. G., Balijepalli, A., Gupta, S. K., and LeBrun, T. W., 2009, "Generating Simplified Trapping Probability Models From Simulation of Optical Tweezers System," J. Comput. Information Sci. Eng., **9**, p. 021003.
[3] Koss, B., Chowdhury, S., Aabo, T., Losert, W., and Gupta, S. K., 2011, "Indirect Optical Gripping With Triplet Traps," J. Opt. Soc. Am. B, **28**(5), pp. 982–985.
[4] Banerjee, A. G., Chowdhury, S., Losert, W., and Gupta, S. K., 2011, "Survey on Indirect Optical Manipulation of Cells, Nucleic Acids, and Motor Proteins," J. Biomed. Opt., **16**(5), p. 051302.
[5] Chowdhury, S., Svec, P., Wang, C., Losert, W., and Gupta, S., 2012, "Gripper Synthesis for Indirect Manipulation of Cells Using Holographic Optical Tweezers," IEEE International Conference on Robotics and Automation, pp. 2749–2754.
[6] Chowdhury, S., Thakur, A., Wang, C., Svec, P., Losert, W., and Gupta, S. K., 2012, "Automated Indirect Transport of Biological Cells With Optical Tweezers Using Planar Gripper Formations," IEEE International Conference on Automatated Scientific Engineering.
[7] Thakur, A., Chowdhury, S., Wang, C., Svec, P., Losert, W., and Gupta, S. K., 2012, "Automated Indirect Optical Micromanipulation of Biological Cells Using Indirect Pushing for Minimizing Photo-Damage," in Proceedings of the ASME Int. Des. Eng. Tech. Conf. and Comp. Inf. Eng. Conf.
[8] Grier, D. G., 2003, "A Revolution in Optical Manipulation," Nature, **424**, pp. 810–816.
[9] Banerjee, A. G., Pomerance, A., Losert, W., and Gupta, S. K., 2010, "Developing a Stochastic Dynamic Programming Framework for Optical Tweezer-Based Automated Particle Transport Operations," IEEE Trans. Autom. Sci. Eng., **7**(2), pp. 218–227.
[10] Banerjee, A. G., Chowdhury, S., Losert, W., and Gupta, S. K., 2012, "Real-Time Path Planning for Coordinated Transport of Multiple Particles Using Optical Tweezers," IEEE Trans. Automat. Sci. Eng., **9**(4), Oct., pp. 669–678.
[11] Chowdhury, S., Svec, P., Wang, C., Seale, K., Wikswo, J. P., Losert, W., and Gupta, S. K., 2011, "Investigation of Automated Cell Manipulation in Optical Tweezers-Assisted Microfluidic Chamber Using Simulations," in Proceedings of the ASME Int. Des. Eng. Tech. Conf. and Comp. Inf. Eng. Conf.
[12] Chowdhury, S., Svec, P., Wang, C., Seale, K., Wikswo, J. P., Losert, W., and Gupta, S. K., 2012, "Automated Cell Transport in Optical Tweezers-Assisted Microfluidic Chambers," IEEE Trans. Automat. Sci. Eng. (to be published).
[13] Chowdhury, S., Thakur, A., Wang, C., Svec, P., Losert, W., and Gupta, S. K., 2013, "Automated Indirect Manipulation of Irregular Shaped Cells With Optical Tweezers for Studying Collective Cell Migration," IEEE International Conference on Robotics and Automation, Karlsruhe, Germany, May 6–10.
[14] Chowdhury, S., Thakur, A., Wang, C., Svec, P., Losert, W., and Gupta, S. K., 2013, "Automated Manipulation of Biological Cells Using Gripper Formations Controlled by Optical Tweezers," IEEE Trans. Automat. Sci. Eng. (to be published).
[15] Ashkin, A., Dziedzic, J. M., Bjorkholm, J. E., and Chu, S., 1986, "Observation of a Single-Beam Gradient Force Optical Trap for Dielectric Particles," Opt. Lett., **11**(5), pp. 288–290.
[16] Bianchi, S., and Leonardo, R. D., 2010, "Real-Time Optical Micro-Manipulation Using Optimized Holograms Generated on the GPU," Comput. Phys. Commun., **181**(8), pp. 1444–1448.
[17] Balijepalli, A., LeBrun, T., and Gupta, S. K., 2010, "Stochastic Simulations With Graphics Hardware: Characterization of Accuracy and Performance," J. Comput. Information Sci. Eng., **10**, p. 011010.
[18] Patro, R., Dickerson, J. P., Bista, S., Gupta, S. K., and Varshney, A., 2012. "Speeding Up Particle Trajectory Simulations Under Moving Force Fields Using GPUs," ASME J. Comput. Information Sci. Eng., **12**(2), p. 021006.
[19] Sraj, I., Szatmary, A. C., Marr, D. W. M., and Eggleton, C. D., 2010, "Dynamic Ray Tracing for Modeling Optical Cell Manipulation," Opt. Express, **18**(16), pp. 16702–16714.
[20] Zhou, J.-H., Ren, H.-L., Cai, J., and Li, Y.-M., 2008, "Ray-Tracing Methodology: Application of Spatial Analytic Geometry in the Ray-Optic Model of Optical Tweezers," Appl. Opt., **47**, pp. 6307–6314.
[21] Harris, M. J., Coombe, G., Scheuermann, T., and Lastra, A., 2002, "Physically-Based Visual Simulation on Graphics Hardware," in Proceedings of the ACM SIGGRAPH/EUROGRAPHICS Conference on Graphics Hardware, HWWS'02, Eurographics Association, pp. 109–118.
[22] Owens, J. D., Luebke, D., Govindaraju, N., Harris, M., Krüger, J., Lefohn, A. E., and Purcell, T., 2007, "A Survey of General-Purpose Computation on Graphics Hardware," Computer Graphics Forum, **26**(1), pp. 80–113.
[23] Harris, M., 2005, "Fast Fluid Dynamics Simulation on the GPU," In SIGGRAPH'05: ACM SIGGRAPH 2005 Courses, ACM, p. 220.
[24] Li, W., Wei, X., and Kaufman, A. E., 2003, "Implementing Lattice Boltzmann Computation on Graphics Hardware," The Visual Computer, **19**(7–8), pp. 444–456.
[25] Liu, Y., Liu, X., and Wu, E., 2004, "Real-Time 3D Fluid Simulation on GPU With Complex Obstacles," in Pacific Conference on Computer Graphics and Applications, IEEE Computer Society, pp. 247–256.
[26] Wei, X., Zhao, Y., Fan, Z., Li, W., Qiu, F., Yoakum-Stover, S., and Kaufman, A. E., 2004, "Lattice-Based Flow Field Modeling," IEEE Trans. Visualization and Computer Graphics, **10**(6), pp. 719–729.
[27] Phillips, E. H., Zhang, Y., Davis, R. L., and Owens, J. D., 2009, "Rapid Aerodynamic Performance Prediction on A Cluster of Graphics Processing Units," AIAA Aerospace Sciences Meeting, No. AIAA 2009-565.
[28] Carr, N. A., Hoberock, J., Crane, K., and Hart, J. C., 2006, "Fast GPU Ray Tracing of Dynamic Meshes Using Geometry Images," Graphics Interface, Canadian Human-Computer Communications Society, pp. 203–209.
[29] Purcell, T. J., Buck, I., Mark, W. R., and Hanrahan, P., 2002, "Ray Tracing on Programmable Graphics Hardware," ACM Trans. Graphics, **21**(3), pp. 703–712.
[30] Fujimoto, A., Tanaka, T., and Iwata, K., 1986, "Arts: Accelerated Ray-Tracing System," IEEE Computer Graphics and Applications, **6**, pp. 16–26.
[31] Lawrence, J., Rusinkiewicz, S., and Ramamoorthi, R., 2004, "Efficient BRDF Importance Sampling Using a Factored Representation," ACM Trans. Graphics, **23**, pp. 496–505.
[32] Singer, W., Bernet, S., and Ritsch-Marte, M., 2001, "3D-Force Calibration of Optical Tweezers for Mechanical Stimulation of Surfactant-Releasing Lung Cells," Laser Phys., **11**(11), pp. 1217–1223.